



Cite this: *Analyst*, 2018, **143**, 3107

## A fast-responsive fluorescent probe for sensitive detection of graphene oxide based on MoS<sub>2</sub> quantum dots†

Haiyan Cao, \*<sup>‡a</sup> Yu Huang, <sup>‡b</sup> Yuanyang Xie,<sup>b</sup> Wenbing Shi,<sup>\*a</sup> Cuicui Fu<sup>a</sup> and Wei He<sup>a</sup>

Facile preparation of water soluble and fluorescent N-doped MoS<sub>2</sub> quantum dots (N-MoS<sub>2</sub> QDs) is described herein. N was introduced to reduce defects in the MoS<sub>2</sub> surface. The obtained N-MoS<sub>2</sub> QDs exhibited excellent fluorescence characteristics with good photostability and excellent stability even in 3 M NaCl solution and when stored in a refrigerator for one year. Additionally, the fluorescent N-MoS<sub>2</sub> QDs were developed as a simple and practical nanosensor for the detection of GO through hydrophobic  $\pi$ - $\pi$  interactions between N-MoS<sub>2</sub> QDs and GO, where the excited state electron and energy transfer may occur from N-MoS<sub>2</sub> QDs to GO along with fluorescence quenching of N-MoS<sub>2</sub> QDs. These results reveal that the limit of detection (LOD) was as low as 4 ng mL<sup>-1</sup>, which was able to satisfy the needs of the determination of GO in environmental water samples. Importantly, the N-MoS<sub>2</sub> QDs nanosensor exhibits excellent detection selectivity against other ions or molecules in the environment. In this study, the proposed sensor was successfully used for the determination of GO content in environmental water samples.

Received 8th May 2018,  
Accepted 22nd May 2018

DOI: 10.1039/c8an00849c

rsc.li/analyst

## Introduction

The development of nanomaterials for various applications is a tremendously challenging task owing to their structure and properties. The ongoing utilization of nanomaterials has caused an increase in their widespread release into the environment.<sup>1</sup> It is reported in the literature that graphene production reached 573 tons in 2017.<sup>2</sup> In this context, there are growing concerns about the possible adverse impact of nanoparticles exposed to terrestrial and aquatic ecosystems. To date, a few studies have revealed that traditional semiconductor quantum dots (QDs), such as CdTe QDs and CdS QDs, as well as metal nanoparticles (M-NPs) posed higher toxicities to human health and the environment in comparison to metal ions of the same elements.<sup>3,4</sup> Only in recent years, graphene and graphene oxide (GO), as one of the most popular nanomaterials, have been shown to induce macrophagic cell

death through oxidative stress and altering cell morphology.<sup>5–7</sup> Moreover, previous studies have proposed that GO can easily accumulate in organs such as lungs, spleen, and liver, leading to toxicity to humans and animals.<sup>8</sup> Although some established methodologies for the detection of M-NPs<sup>9,10</sup> or carbon nanotubes<sup>11,12</sup> have been reported, practically there are few analytical tools<sup>13,14</sup> for the quantification of concentrations of GO in environmental samples. Thus, the design of more effective methods for the detection of graphene oxide in the environment is essential and urgently needed.

Fluorescence methods have attracted increasing attention because of their simplicity, sensitivity and rapidity.<sup>15–23</sup> Recently, Sandra *et al.*<sup>13</sup> reported water-soluble fluorescent graphene quantum dots for the detection of GO with detection limit (LOD) of 35  $\mu\text{g L}^{-1}$ . Another study on detecting GO was based on  $\beta$ -cyclodextrin-protected Cu nanoclusters (LOD = 100.0  $\mu\text{g L}^{-1}$ ).<sup>14</sup> Established analytical tools for GO quantification are not suitable for directly detecting GO in the environment since in most cases, the dissolved GO in the environment in a complex mixture is present in extremely low concentration ( $\mu\text{g L}^{-1}$  range).<sup>13</sup> Therefore, a more sensitive, simple, eco-friendly, and selective sensor strategy for sensing of trace levels of GO in complex environmental samples is necessary and is an emerging topic of research.

Molybdenum disulfide (MoS<sub>2</sub>), recently demonstrated as a layered transition-metal dichalcogenide material, has attracted much attention due to its unique structure and electronic pro-

<sup>a</sup>The Key Laboratory of Chongqing Inorganic Special Functional Materials, College of Chemistry and Chemical Engineering, Yangtze Normal University, Chongqing 408100, China. E-mail: 513923170@qq.com, wenbingshi@hotmail.com; Fax: +86-23-68254843; Tel: +86-23-68254843

<sup>b</sup>Chongqing Institute of Green and Intelligent Technology, Chinese Academy of Sciences, Chongqing 400714, China

†Electronic supplementary information (ESI) available. See DOI: 10.1039/c8an00849c

‡These authors contributed equally to this work.

erties.<sup>24</sup> In particular, single-layer MoS<sub>2</sub> materials exhibit excellent tunable photoluminescence properties<sup>25</sup> with many advantages including low toxicity, good water solubility, high fluorescent activity, robust chemical inertness, excellent photostability, and high thermal stability. MoS<sub>2</sub>-based fluorescent sensors offer numerous opportunities to develop new and ideal methodologies for biomolecules, metal ions, nucleic acids, and small molecules detection.<sup>26</sup> Consequently, various strategies have been explored for the preparation of single or few-layer MoS<sub>2</sub> nanosheets, which mainly include “top-bottom” stripping<sup>27–29</sup> and “bottom-top” hydrothermal methods.<sup>30,31</sup> However, the defects of uncontrolled dopants, charge carrier traps and nonradiative recombination centers are reported in MoS<sub>2</sub> monolayers and have held back widespread research on their potential applications. Some approaches, such as molecular oxygen treatment, ionic liquid adsorption, and substrate deactivation, have been adopted to reduce the defects in MoS<sub>2</sub> surfaces.<sup>32,33</sup> Chemical doping in nanomaterials could also effectively tune their electronic properties and chemical activity. Because of this fact, Feng *et al.* have reported MoS<sub>2</sub> nanosheets co-doped with boron and nitrogen, which exhibit enhanced fluorescence and can be used for the selective and sensitive detection of Hg<sup>2+</sup> ions.<sup>34</sup> N-doped carbon materials have been widely reported. Nevertheless, the reports on N-doped MoS<sub>2</sub> are still scarce due to the lack of synthesis techniques.

In this report, a simple and innovative approach for large-scale production of N-doped MoS<sub>2</sub> quantum dots (N-MoS<sub>2</sub> QDs) is proposed, which involves the addition of glutathione as the nitrogen and sulfur source *via* a one-step and green hydrothermal method. The as-synthesized N-MoS<sub>2</sub> QDs exhibited blue emission at 410 nm with a quantum yield (QY) of 13.1%, excellent stability, resistance to photobleaching, and good water solubility. Notably, N-MoS<sub>2</sub> QDs serve as a rapid fluorescent probe for the determination of GO in environmental samples with high selectivity. This strategy was based on the fact that excited state electron and energy transfer may occur from N-MoS<sub>2</sub> QDs to GO along with the fluorescence quenching of N-MoS<sub>2</sub> QDs. The analytical procedure does not involve any complex chemical synthesis or complicated operations. More importantly, the proposed method is capable of satisfying the needs of the determination of GO dissolved in environmental water sources with a detection limit as low as 4 ng mL<sup>-1</sup>. These N-MoS<sub>2</sub> QDs have great potential to be applied as environmental sensors.

## Experimental section

### Chemicals and reagents

All chemicals and reagents were of analytical grade and used as received from commercial suppliers. Glutathione (GSH) was obtained from Aladdin Ltd (Shanghai, China). HCl and NaOH were supplied from Macklin Inc. (Shanghai, China). Graphene oxide (GO) (Thickness, 0.55–1.2 nm; length, 0.5–3 μm; purity, >99%) was purchased from Beijing Island Gold Deco

Technology Co. Ltd (Beijing, China). Single walled carbon nanotubes (SWCNT) (OD, <8 nm; length, 30 μm; purity, >95%) and multi-walled carbon nanotubes (MWCNT) (OD, <8 nm; length, 30 μm; purity, >95%) were obtained from Chengdu Organic Chemicals Co. Ltd, Chinese Academy of Sciences (Chengdu, China). Sodium molybdate dihydrate (NaMoO<sub>4</sub>·2H<sub>2</sub>O), hydrazine hydrate and polyethylene glycol (PEG) were purchased from Sigopharm Chemical Reagent Co., Ltd (Shanghai, China). Ultrapure water was used throughout the study and prepared in the lab using a water treatment device.

### Instrumentation

The fluorescence and absorption spectra were recorded on a Hitachi F-7000 Fluorescence spectrophotometer (Kyoto, Japan) and a model UV-2450 spectrophotometer (Shimadzu, Japan), respectively. The FTIR spectrum of N-MoS<sub>2</sub> QDs was obtained using an Agilent Cary 630 spectrometer. pH of the solutions were recorded using a PHS-3D pH meter (Shanghai Precision Scientific Instruments Co., Ltd, China). Dynamic light scattering (DLS) was carried out using a Malvern Instruments Zetasizer Nano-ZS (Malvern, UK) instrument for characterization of the size distribution of the N-MoS<sub>2</sub> QDs in solution. The morphology of the nanomaterials was observed using a transmission electron microscope (TEM, LIBRA 200, ZEISS) at an acceleration voltage of 200 kV. The atomic force microscopy (AFM) measurements were carried out on a Nanoscope IIIa (Digital Instrument, USA) under tapping mode, and the Raman spectrometer analysis was performed on an in Via-Reflex Confocal Raman spectrometer (Renishaw, UK). X-ray photoelectron spectroscopy (XPS) spectra were measured by an XSAM-800 X-ray photoelectron spectroscope (KRATOS, Britain).

### Synthesis of N-doped MoS<sub>2</sub> quantum dots

To NaMoO<sub>4</sub>·2H<sub>2</sub>O (0.25 g) in ultrapure water (60 mL), GSH (0.3 g) was added under ultrasound for 10 min. Subsequently, the solution was transferred into a 100 mL PTFE autoclave high pressure vessel, and then heated at 200 °C in an oven for 45 hours. After cooling to room temperature, the mixture was centrifuged for 10 min at 14 000 rpm. The obtained supernatant was dialyzed by a dialysis membrane (MWCO: 7000 Da; pore size: *ca.* 0.7 nm) to separate the N-doped MoS<sub>2</sub> quantum dots (N-MoS<sub>2</sub> QDs) from any residual unreacted species. The as-purified N-MoS<sub>2</sub> QDs were characterized by TEM, XPS, DLS, FT-IR and UV-Vis spectroscopy and stored at 4 °C until required for further use (stable for at least twelve months). The mass concentration of the N-MoS<sub>2</sub> QDs was calculated to be 3113 mg L<sup>-1</sup> by weighing the reagent bottles containing dried residue and subtracting the quality of the empty reagent bottles.

### Fluorescence spectroscopic analysis

Various concentrations of GO (range, C<sub>GO</sub> = 0–20 μg mL<sup>-1</sup>) were added to the solution consisting of N-MoS<sub>2</sub> QDs (final concentration of 18.7 mg L<sup>-1</sup>) in such a way that the desired final concentration of GO in the solution was obtained. The

solutions were mixed thoroughly and then incubated at room temperature for 5 minutes. Subsequently, they were transferred into a cuvette and the corresponding FL spectra and FL signal were recorded. The relative fluorescence intensity  $[(I_0 - I)/I]$  versus GO concentration was used for calibration, where,  $I_0$  and  $I$  are the fluorescence intensities of the N-MoS<sub>2</sub> QDs before and after the addition of GO, respectively. At each GO concentration, the measurement was repeated three times, and the average FL signal was obtained.

### Procedure for GO determination in water samples

In this study, river water samples were selected for investigation. River water was collected from the Jialing River in the upper reaches of the Three Gorges Reservoir area. The environmental water samples were filtered through 0.45  $\mu\text{m}$  acetate of cellulose membranes and then, 1 mL of a 0.25 mol L<sup>-1</sup> NaOH solution was passed through the filter membrane for eliminating the interference of organic substances in the environmental sample. Later, 1 mL of ultrapure water was passed through the membrane. Finally, the membrane with 200  $\mu\text{L}$  of ultrapure water was treated by ultrasound for 40 s in order to recover the graphene oxide from the membrane, and subsequently used for GO analysis. In a typical process, the obtained sample was added to the solution consisting of N-MoS<sub>2</sub> QDs (final concentration of 18.7 mg L<sup>-1</sup>), and then subjected to fluorescence determination. For the recovery test, the spiked environmental water samples with different levels of GO were used. The recovery was calculated as the ratio of the amount of recovered GO to that of the spiked GO. Determinations were performed in triplicate for three preparations of water samples.

## Results and discussion

### Synthesis and characterization of N-doped MoS<sub>2</sub> quantum dots

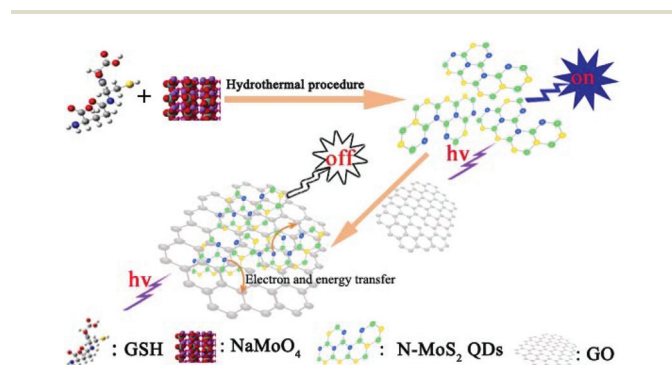
N-doped MoS<sub>2</sub> quantum dots (N-GQDs) were synthesized through a facile hydrothermal procedure involving the overall formation process shown in Scheme 1, where glutathione was

used as both nitrogen and sulfur source. Typically, glutathione was utilized for introducing N-atoms into the MoS<sub>2</sub> lattice through the high temperature hydrothermal process. Clearly, the entire process is easily carried out and environmentally friendly.

Dynamic light scattering (DLS) measurements of the N-MoS<sub>2</sub> QDs showed the formation of non-aggregated N-MoS<sub>2</sub> QDs having a size of less than 2 nm (Fig. ESI-1A†). Moreover, HRTEM images (Fig. 1a) confirmed the monodispersity of the as-obtained N-MoS<sub>2</sub> QDs (average diameter:  $2.7 \pm 0.6$  nm). The zeta potential of the N-MoS<sub>2</sub> QDs was determined to be  $-22.4$  mV (Fig. ESI-1B†), suggesting great colloidal stability in aqueous media.

Raman spectroscopy can provide a reliable and convenient means for identifying the layer thickness of MoS<sub>2</sub>-based materials.<sup>24</sup> As shown in Fig. 1b, two characteristic Raman modes on the sample at around 383.5 and 399.8 cm<sup>-1</sup>, which are attributed to the in-plane vibrational E<sub>2g</sub><sup>1</sup> mode and the out-of-plane vibrational A<sub>1g</sub> mode, respectively, were consistent with that of monolayers of MoS<sub>2</sub> QDs reported previously.<sup>35–37</sup> The layer assignment was confirmed by atomic force microscopy (AFM). As revealed by atomic force microscopy (AFM) analysis (inset of Fig. 1c), the average thickness of the N-MoS<sub>2</sub> QDs was  $1.08 \pm 0.17$  nm (the height was statistically calculated from more than 50 QDs in the AFM images).

FT-IR spectrum was recorded to clarify the surface state of the MoS<sub>2</sub> QDs. The FT-IR spectrum shown in Fig. ESI-2† displayed several peaks of the oxygen and nitrogenous functionalities, including peaks at 1381 cm<sup>-1</sup> and 1659 cm<sup>-1</sup> that resulted from the deformation of C–O in the carboxyl group and the N–H bending vibration, respectively,<sup>38–40</sup> and the broad peak at 3324 cm<sup>-1</sup> from O–H vibration<sup>37</sup> and N–H stretching vibration.<sup>39</sup> The peak at 2974 cm<sup>-1</sup> was assigned to the C–H stretching vibration.<sup>41</sup> Notably, the peak at 1048 cm<sup>-1</sup> corresponded to the N in-plane bending vibration, which is consistent with that of other N-doped graphene dots (GQDs).<sup>38</sup>



**Scheme 1** Schematic illustration for the preparation of water-soluble fluorescent N-MoS<sub>2</sub> QDs and the detection of GO with N-MoS<sub>2</sub> QDs as a nanosensor.

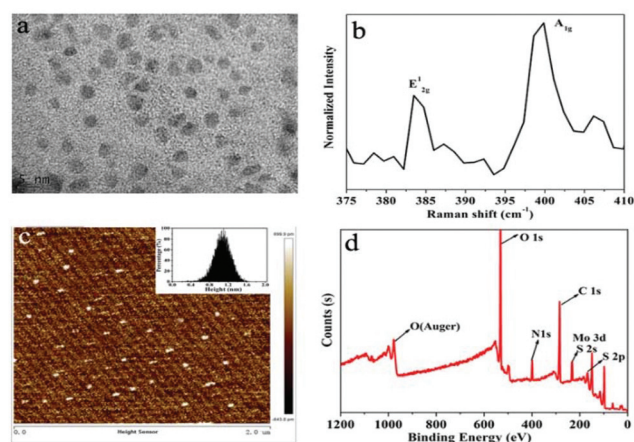


**Fig. 1** (a) HRTEM images of N-MoS<sub>2</sub> QDs (scale bar corresponds to 5 nm); (b) Raman spectra of N-MoS<sub>2</sub> QDs; (c) AFM images of N-MoS<sub>2</sub> QDs; (d) XPS spectrum of N-MoS<sub>2</sub> QDs.



indicating that N-MoS<sub>2</sub> QDs were successfully obtained. Also, the weak absorption peak at 465 cm<sup>-1</sup> was attributed to the fingerprint characteristic of MoS<sub>2</sub>.<sup>37</sup> These results indicate that N had been conjugated onto the surface of the MoS<sub>2</sub> QDs. The XPS results (shown in Fig. 1d) further confirm the stability of the nitrogen species in the MoS<sub>2</sub> QDs structure. In the XPS spectra, the peaks at 164.7, 231.8, 284.7, 399.3 and 531.0 eV corresponded to S 2p, Mo 3d, C 1s, N 1s and O 1s, respectively. Furthermore, a total nitrogen concentration of ~10.93% was obtained for the N-MoS<sub>2</sub> QDs. The N 1s core level XPS spectra of the N-MoS<sub>2</sub> QDs (see Fig. ESI-3†) exhibited three grouped peaks attributed to Mo–N, the N in the aromatic ring (N<sub>ar</sub>) and pyrrolic N centred at the binding energy values of 397.7, 399.3 and 400.1 eV, respectively, which was in agreement with the results from other reports.<sup>41–44</sup> Thus, all of the above results confirmed that ultrasmall sized N-MoS<sub>2</sub> QDs materials had been prepared successfully using the proposed method, and they were homogeneous in size with narrow size distribution.

UV-Vis absorption spectroscopy has been used as a powerful and convenient diagnostic tool to study the electronic structure of quantum dots. Such molecular-like properties were also observed for the N-MoS<sub>2</sub> QDs synthesized in this study. The distinct peak at about 300 nm assigned to the excitonic features of MoS<sub>2</sub> QDs appeared in the UV-Vis absorption spectra of the N-MoS<sub>2</sub> QDs (in black line from Fig. 2), and was associated with the presence of peaks of other synthesized MoS<sub>2</sub> QDs.<sup>45</sup> The as-synthesized N-MoS<sub>2</sub> QDs showed significantly different optical transition absorbance bands compared to bulk MoS<sub>2</sub>; the typical UV-Vis absorption peak for bulk MoS<sub>2</sub> (*ca.* 620 and 670 nm attributed to the *K* point of the Brillouin zone<sup>46</sup>) disappeared due to the quasi-continuous electronic energy band structure and quantum confinement effects. The photoluminescence (PL) emission and excitation spectra are shown as the red lines in Fig. 2. In aqueous solution, the N-MoS<sub>2</sub> QDs showed maximum emission located at 410 nm when they were excited at 340 nm. QY of 13.1% against the reference of quinine sulphate was produced, which is higher than that of most previously reported fluorescent graphene QDs or MoS<sub>2</sub> QDs.<sup>31,47–49</sup> It is clearly observed from the

inset images of Fig. 2 that the N-MoS<sub>2</sub> QDs exhibit flaxen solution color under irradiation from sunlight (left image), while N-MoS<sub>2</sub> QDs exhibit a bright blue fluorescence color under irradiation from a 302 nm lamp (right image).

In order to confirm the stability of the N-MoS<sub>2</sub> QDs, their fluorescence spectra were measured in a solution containing different concentrations of NaCl. As shown in Fig. ESI-4,† a slight change in the fluorescence intensity revealed that the N-MoS<sub>2</sub> QDs were stable under conditions of high ionic strength or oxidation in 3 M NaCl solution and 150 μM H<sub>2</sub>O<sub>2</sub>, respectively. This finding suggests that N-MoS<sub>2</sub> QDs have great potential for sensing molecules under high ionic strength and oxidizing environments. It can be seen in Fig. ESI-6A† that the emission peak intensity of the N-MoS<sub>2</sub> QDs remains unchanged at pH values from 4 to 9, indicating that the N-MoS<sub>2</sub> QDs could work in environments and biosystems with a wide range of pH. Moreover, the photostability of the N-MoS<sub>2</sub> QDs was characterized. The fluorescence intensity of N-MoS<sub>2</sub> QDs in aqueous or 98% (v/v) methanol remained almost unchanged after 30 min of continuous irradiation, suggesting that they have good photostability (Fig. ESI-5A†). Furthermore, it was demonstrated that water-soluble N-MoS<sub>2</sub> QDs had better fluorescence properties. Moreover, the N-MoS<sub>2</sub> QDs presented good stability. No distinct change in the fluorescence intensity could be found when the N-MoS<sub>2</sub> QDs were stored at 4 °C for more than one year (Fig. ESI-5B†).

The cytotoxicity of N-MoS<sub>2</sub> QDs was examined by the cell-counting kit-8 (CCK-8, Dojindo Laboratories, Japan) assay.<sup>50,51</sup> First, HO-8910 cells were seeded in 96-well plates at a density of  $3.25 \times 10^4$  cells per mL. After 24 h incubation, the medium was replaced with a medium containing N-MoS<sub>2</sub> QDs of various concentrations (0, 1, 6, 15, 20, 25, 50 and 100 mg L<sup>-1</sup>), and the cells were incubated for another 24 h. Next, the cells were washed thrice with phosphate buffered saline (PBS), and freshly prepared CCK-8 (10 μL) solution in a culture medium (90 μL) was added to each well. After 2 h incubation, the CCK-8 medium solution was carefully removed. Then, the plate was gently shaken for 10 min at room temperature, and the optical density (OD) of the mixture was measured at 450 nm. The cell viability was assessed by the following equation: Cell viability (%) = (Sample OD – Blank OD) / (Control OD – Blank OD) × 100%. As shown in Fig. ESI-9,† almost 100% of HO-8910 cells are alive in the concentration ranges of the N-MoS<sub>2</sub> QDs used in our experiments. Thus, N-MoS<sub>2</sub> QDs show very low cytotoxicity and are suitable for the detection of GO in the environment. The application of this nanomaterials probe for detecting GO can be extended to biological systems.

### Graphene oxide detection

GO has been widely used as an energy receptor in fluorescence resonance energy transfer (FRET) applications as a result of nonradiative transfer of electronic excitation energy from dye, quantum dots or metal nanoclusters excited states to its  $\pi$ -system.<sup>52–55</sup> Despite the numerous applications of FRET based on GO, it remains an underdeveloped analytical tool for

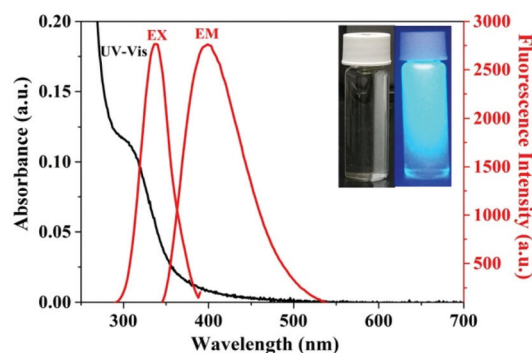


Fig. 2 UV absorption spectra (black line) and fluorescence spectra (red line) of N-MoS<sub>2</sub> QDs; the inset is a photograph of the N-MoS<sub>2</sub> QDs under irradiation from visible light (left) and 302 nm light (right).

the quantification of concentrations of GO. Inspired by this property, we constructed a fluorescence method for GO detection using N-MoS<sub>2</sub> QDs (shown in Scheme 1), which is attributed to the presence of excited state electrons and the energy transfer process from MoS<sub>2</sub> QDs to GO.<sup>56</sup>

To obtain the optimum conditions of the detection system, the effect of pH on the fluorescence response of the N-MoS<sub>2</sub> QDs to GO was investigated. As shown in Fig. ESI-6A,<sup>†</sup> the fluorescence intensity showed no high variations over a wide pH range of 4.0–9.0 both in the absence and presence of GO. Hence, no change in the relative fluorescence intensity  $[(I_0 - I)/I]$  was observed over a wide pH range of 4.0–9.0, indicating that the sensor is promising for environmental and biological applications without pH adjustment. We studied the kinetic behaviour of the interaction between N-MoS<sub>2</sub> QDs and GO through hydrophobic  $\pi$ - $\pi$  interactions in aqueous and 98% (v/v) methanol. As shown in Fig. ESI-6B,<sup>†</sup> the FL intensity at 410 nm of the N-MoS<sub>2</sub> QDs increases drastically during the early stages of the reaction and reaches a plateau after less than 2 min, which demonstrates that GO can selectively and rapidly bind with the N-MoS<sub>2</sub> QDs surfaces at room temperature in aqueous solution. Thus, 2 min was chosen as the reaction time in aqueous solution and 10 min was chosen as the reaction time in 98% methanol. Furthermore, both water and a 98% (v/v) methanol solution were assayed. The effect of the concentrations of N-MoS<sub>2</sub> QDs on the detection of GO was studied. From Fig. ESI-6C,<sup>†</sup> it was observed that the maximum value of the relative fluorescence intensity  $[(I_0 - I)/I]$  under the conditions of the same amount of GO at 18.68 mg L<sup>-1</sup> N-MoS<sub>2</sub> QDs. Thus, the optimal N-MoS<sub>2</sub> QD concentration of 18.68 mg L<sup>-1</sup> was chosen for GO detection.

Under the optimal conditions, different concentrations of GO (0.05–20  $\mu\text{g mL}^{-1}$ ) were added to 18.68 mg L<sup>-1</sup> N-MoS<sub>2</sub> QDs. It can be seen from Fig. 3A that the decrease in fluorescence intensity of N-MoS<sub>2</sub> QDs occurs with an increase in the concentration of GO. Moreover, a linear relationship was observed between the relative fluorescence intensity  $[(I_0 - I)/I]$  of N-MoS<sub>2</sub> QDs and the concentration of GO from 0.05 to 20  $\mu\text{g mL}^{-1}$  (Fig. 3B). The regression equation could be expressed as  $(I_0 - I)/I = 0.0727 + 0.0384 [\text{GO}] (\mu\text{g mL}^{-1})$ ,  $R^2 = 0.9962$  ( $n = 12$ ). The RSD was 3.09% for 10  $\mu\text{g mL}^{-1}$  GO ( $n = 11$ ). The limit of detection (LOD) for GO at a signal-to-noise

ratio of 3 was estimated to be 4 ng mL<sup>-1</sup>, which was capable of satisfying the needs of the determination of GO in environmental water samples, in which the level of GO is in the low concentration of ng mL<sup>-1</sup> range.<sup>13</sup> Furthermore, the present method was compared to the analytical methods previously published in the literature<sup>13,14</sup> using fluorescence spectrum for GO analysis in terms of LODs, which are based on graphene quantum dots and  $\beta$ -cyclodextrin protected Cu nanoclusters. The LOD obtained in this study was one or two orders of magnitude lower than that of the previous reports, thus demonstrating the high sensitivity of the proposed method for detecting GO. Herein, we also carried out detection studies with other common metal ions, anions, and molecules in complex environmental water samples, such as Ca<sup>2+</sup>, K<sup>+</sup>, Na<sup>+</sup>, Mg<sup>2+</sup>, Al<sup>3+</sup>, Cd<sup>2+</sup>, Cu<sup>2+</sup>, Hg<sup>2+</sup>, Co<sup>2+</sup>, Pb<sup>2+</sup>, Cr<sup>3+</sup>, Ni<sup>2+</sup>, Mn<sup>2+</sup>, Fe<sup>3+</sup>, Zn<sup>2+</sup>, Cl<sup>-</sup>, NO<sub>3</sub><sup>-</sup>, SO<sub>4</sub><sup>2-</sup>, CO<sub>3</sub><sup>2-</sup>, urea, single walled carbon nanotubes (SWCNT), multi-walled carbon nanotubes (MWCNT), reduced Graphene Oxide (rGO) and polyethylene glycol-modified graphene oxide (PEG-GO) under exactly similar conditions that were used for the detection of GO. The results demonstrated that all of the tested cations, anions, molecule, SWCNT, MWCNT and rGO have no evident effect on the fluorescence intensity of the N-MoS<sub>2</sub> QDs, while PEG-GO causes fluorescence quenching (Fig. ESI-7<sup>†</sup>). Thus, the results indicate good selectivity of this sensing method towards GO and other modified GO. Clearly, due to its luminescence, the as-prepared N-MoS<sub>2</sub> QDs can be used as a highly sensitive and selective luminescence “turn-off” sensor for GO and other modified GO in environmental samples.

## Application

To explore the anti-interference abilities of the N-MoS<sub>2</sub> QDs for the detection of GO, the effect of coexisting metal ions, anions or small molecules on the quenched fluorescence intensity of the N-MoS<sub>2</sub> QDs by GO was tested. In these experiments, we analysed standard solutions of GO (5  $\mu\text{g mL}^{-1}$ ), to which 5  $\mu\text{g mL}^{-1}$  of metal ions, anions or small molecules, including Ca<sup>2+</sup>, K<sup>+</sup>, Na<sup>+</sup>, Mg<sup>2+</sup>, Al<sup>3+</sup>, Cd<sup>2+</sup>, Cu<sup>2+</sup>, Hg<sup>2+</sup>, Co<sup>2+</sup>, Pb<sup>2+</sup>, Cr<sup>3+</sup>, Ni<sup>2+</sup>, Mn<sup>2+</sup>, Fe<sup>3+</sup>, Zn<sup>2+</sup>, Cl<sup>-</sup>, NO<sub>3</sub><sup>-</sup>, SO<sub>4</sub><sup>2-</sup>, CO<sub>3</sub><sup>2-</sup>, urea, single walled carbon nanotubes (SWCNT) and multi-walled carbon nanotubes (MWCNT), were added. As shown in Fig. ESI-8,<sup>†</sup> the interference of 5  $\mu\text{g mL}^{-1}$  foreign ions or small molecules to 5  $\mu\text{g mL}^{-1}$  of GO were between 0.3% and 2.7%. These results indicate good anti-interference abilities of this sensing method towards GO. The applicability of the proposed method for detecting GO in real environmental samples was further

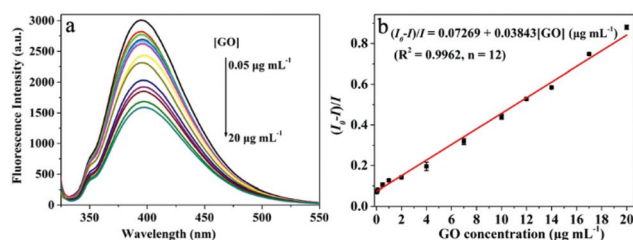


**Fig. 3** (a) Fluorescence responses of N-MoS<sub>2</sub> QDs after the addition of GO (0, 0.05, 0.1, 0.5, 1, 2, 4, 7, 10, 12, 14, 17, 20  $\mu\text{g mL}^{-1}$ ); (b) plots of the values of  $(I_0 - I)/I$  versus the concentrations of GO. The error bars represent standard deviations based on three independent measurements.

**Table 1** Determination results of GO content in environmental samples

River water sample	Added concentration of GO ( $\mu\text{g mL}^{-1}$ )	Found concentration of GO <sup>a</sup> ( $\mu\text{g mL}^{-1}$ )	Recovery (%)
1	0.1	$0.11 \pm 0.01$	107.8
2	0.5	$0.49 \pm 0.04$	98.0
3	1	$1.06 \pm 0.08$	105.5

<sup>a</sup> Determined by the proposed method (average  $\pm$  SD,  $n = 3$ ).

evaluated. Although no graphene oxide was expected to be found in them, recovery tests were carried out on the samples. The results are shown in Table 1. It can be seen that the recovery for spiked water samples was from 98.0 to 107.8%, showing a great potential of the sensor for the routine estimation of GO content in environmental samples.

## Conclusions

In summary, a fluorescence nanosensor for GO detection was designed based on N-MoS<sub>2</sub> QDs. N-MoS<sub>2</sub> QDs were simply synthesized by using glutathione as a nitrogen and sulfur source via a one-step green hydrothermal method. N-MoS<sub>2</sub> QDs exhibited excellent fluorescence characteristics with good photostability and excellent stability even in 3 M NaCl solution and when stored in a refrigerator for one year. Moreover, the obtained N-MoS<sub>2</sub> QDs could recognize GO directly due to the excited state electron and energy transfer from the N-MoS<sub>2</sub> QDs to GO with fluorescence quenching. The measurement of GO is simple and sensitive, and a limit of detection as low as 4 ng mL<sup>-1</sup> was achieved. To the best of our knowledge, this is the first report concerning a sensing approach based on fluorescence quenching for the determination of GO using fluorescent N-MoS<sub>2</sub> QDs. The results confirm the validity of this N-MoS<sub>2</sub> QDs-based FL sensing method for the detection of GO in real environmental samples. For its simplicity and cost effectiveness, we believe that the detection system will have potential applications in the environmental monitoring field.

## Conflicts of interest

There are no conflicts to declare.

## Acknowledgements

The authors gratefully acknowledge the financial support of the National Natural Science Foundation of China (Grant No. 21707137 and 21705009), the Key Application and Development Program of Chongqing (No. cstc2017shmsA0159), Research Funding Project of Yangtze Normal University (No. 2017KYQD23), Young Scientist Research Fund of Yangtze Normal University, Program for Innovation Team Building at Institutions of Higher Education in Chongqing (No. CXTDX201601039) and Scientific and Technological Research Program of Chongqing Municipal Education Commission (No. KJ1401201).

## Notes and references

- 1 S. J. Klaine, P. J. J. Alvarez, G. E. Batley, T. F. Fernandes, R. D. Handy, D. Y. Lyon, S. Mahendra, M. J. McLaughlin and J. R. Lead, *Environ. Toxicol. Chem.*, 2008, **27**, 1825–1851.
- 2 K. S. Sivudu and Y. Mahajan Mass, *Mass production of high quality graphene: An analysis of worldwide patents*, 2012, <http://www.nanowerk.com/spotlight/spotid=25744.php>.
- 3 T. Puzyn, B. Rasulev, A. Gajewicz, X. Hu, T. P. Dasari, A. Michalkova, H. M. Hwang, A. Toropov, D. Leszczynska and J. Leszczynski, *Nat. Nanotechnol.*, 2011, **6**, 175–178.
- 4 A. M. Derfus, W. Chan and S. N. Bhatia, *Nano Lett.*, 2003, **4**, 11–18.
- 5 Y. Chang, S.-T. Yang, J.-H. Liu, E. Dong, Y. Wang, A. Cao, Y. Liu and H. Wang, *Toxicol. Lett.*, 2011, **200**, 201–210.
- 6 K.-H. Liao, Y.-S. Lin, C. W. Macosko and C. L. Haynes, *ACS Appl. Mater. Interfaces*, 2011, **3**, 2607–2615.
- 7 M. Zhang, X. Mao, C. Wang, W. Zeng, C. Zhang, Z. Li, Y. Fang, Y. Yang, W. Liang and C. Wang, *Biomaterials*, 2013, **34**, 1383–1390.
- 8 G. Duan, S. G. Kang, X. Tian, J. A. Garate, L. Zhao, C. Ge and R. Zhou, *Nanoscale*, 2015, **7**, 15214.
- 9 L. Li and K. Leopold, *Anal. Chem.*, 2012, **84**, 4340–4349.
- 10 G. Hartmann, T. Baumgartner and M. Schuster, *Anal. Chem.*, 2014, **86**, 790.
- 11 A. I. Lópezlorente, B. M. Simonet and M. Valcárcel, *Talanta*, 2013, **105**, 75–79.
- 12 Á. I. LópezLorente, M. L. Pololuque and M. Valcárcel, *Anal. Chem.*, 2013, **85**, 10338–10343.
- 13 B. M. Sandra, L. L. Angela Inmaculada and V. Miguel, *Anal. Chem.*, 2015, **86**, 12279.
- 14 Y. Zhong, Y. He, Y. Ge and G. Song, *Luminescence*, 2016, **4**, 596–601.
- 15 Y. Ding, S. Wang, J. Li and L. Chen, *TrAC, Trends Anal. Chem.*, 2016, **82**, 175–190.
- 16 Z. Li, N. Xue, H. Ma, Z. Cheng and X. Miao, *Talanta*, 2018, **181**, 346–351.
- 17 Q. Liu, N. Li, M. Wang, L. Wang and X. Su, *Anal. Chim. Acta*, 2018, **1013**, 71–78.
- 18 Y. Liu, X. Hu, L. Bai, Y. Jiang, J. Qiu, M. Meng, Z. Liu and L. Ni, *Microchim. Acta*, 2018, **185**, 48.
- 19 X. Wang, J. Yu, J. Li, Q. Kang, D. Shen and L. Chen, *Sens. Actuators, B*, 2018, **255**, 268–274.
- 20 X. Wang, J. Yu, X. Wu, J. Fu, Q. Kang, D. Shen, J. Li and L. Chen, *Biosens. Bioelectron.*, 2016, **81**, 438–444.
- 21 J. Yu, X. Wang, Q. Kang, J. Li, D. Shen and L. Chen, *Environ. Sci.: Nano*, 2017, **4**, 493–502.
- 22 N. Yu, H. Peng, H. Xiong, X. Wu, X. Wang, Y. Li and L. Chen, *Microchim. Acta*, 2015, **182**, 2139–2146.
- 23 N. Zhou, J. Li, H. Chen, C. Liao and L. Chen, *Analyst*, 2013, **138**, 1091–1097.
- 24 J. Ping, Z. Fan, M. Sindoro, Y. Ying and H. Zhang, *Adv. Funct. Mater.*, 2017, **27**, 1605817.
- 25 V. Štengl and J. Henych, *Nanoscale*, 2013, **5**, 3387–3394.
- 26 X. Zhang, Z. Lai, C. Tan and H. Zhang, *Cheminform*, 2016, **55**, 8816.
- 27 G. S. Bang, K. W. Nam, J. Y. Kim, J. Shin, J. W. Choi and S. Y. Choi, *ACS Appl. Mater. Interfaces*, 2014, **6**, 7084–7089.
- 28 G. D. Mm and D. D. Shaijumon, *ACS Nano*, 2014, **8**, 5297–5303.

- 29 H. Schmidt, S. Wang, L. Chu, M. Toh, R. Kumar, W. Zhao, A. H. Castro Neto, J. Martin, S. Adam, B. Oezylmaz and G. Eda, *Nano Lett.*, 2014, **14**, 1909–1913.
- 30 Y. Peng, Z. Meng, Z. Chang, J. Lu, W. Yu, Y. B. Jia and Y. Qian, *Chem. Lett.*, 2001, **2001**, 772–773.
- 31 W. Yong and N. Yongnian, *Anal. Chem.*, 2014, **86**, 7463–7470.
- 32 V. P. Pham and G. Y. Yeom, *Adv. Mater.*, 2016, **28**, 9024.
- 33 T. L. Atallah, J. Wang, M. Bosch, D. Seo, R. A. Burke, O. Moneer, J. Zhu, M. Theibault, L. E. Brus and J. Hone, *J. Phys. Chem. Lett.*, 2017, 2148–2152.
- 34 X. Liu, L. Li, Y. Wei, Y. Zheng, Q. Xiao and B. Feng, *Analyst*, 2015, **140**, 4654–4661.
- 35 C. Lee, H. Yan, L. E. Brus, T. F. Heinz, J. Hone and S. Ryu, *ACS Nano*, 2010, **4**, 2695–2700.
- 36 H. Zeng, J. Dai, W. Yao, D. Xiao and X. Cui, *Nat. Nanotechnol.*, 2012, **7**, 490.
- 37 H. Huang, C. C. Du, H. Y. Shi, X. Feng, J. Li, Y. L. Tan and W. B. Song, *Part. Part. Syst. Character.*, 2015, **32**, 72–79.
- 38 T. V. Tam, N. B. Trung, H. R. Kim, S. C. Jin and W. M. Choi, *Sens. Actuators, B*, 2014, **202**, 568–573.
- 39 L. Lai, L. Chen, D. Zhan, L. Sun, J. Liu, S. H. Lim, C. K. Poh, Z. Shen and J. Lin, *Carbon*, 2011, **49**, 3250–3257.
- 40 Y. Hu, X. Geng, L. Zhang, Z. Huang, J. Ge and Z. Li, *Sci. Rep.*, 2017, **7**, 5849.
- 41 D. Deng, X. Pan, L. Yu, Y. Cui, Y. Jiang, J. Qi, W. X. Li, Q. Fu, X. Ma and Q. Xue, *Chem. Mater.*, 2011, **23**, 1188–1193.
- 42 D. Wei, Y. Liu, Y. Wang, H. Zhang, L. Huang and G. Yu, *Nano Lett.*, 2009, **9**, 1752.
- 43 J. Sun, S. Yang, Z. Wang, H. Shen, T. Xu, L. Sun, H. Li, W. Chen, X. Jiang and G. Ding, *Part. Part. Syst. Character.*, 2015, **32**, 434–440.
- 44 R. Sanjinés, C. Wiemer, J. Almeida and F. Lévy, *Thin Solid Films*, 1996, **290–291**, 334–338.
- 45 V. Chikan and D. F. Kelley, *J. Phys. Chem. B*, 2002, **106**, 3794–3804.
- 46 A. Splendiani, L. Sun, Y. Zhang, T. Li, J. Kim, C. Y. Chim, G. Galli and F. Wang, *Nano Lett.*, 2010, **10**, 1271–1275.
- 47 D. Pan, J. Zhang, Z. Li and M. Wu, *Adv. Mater.*, 2010, **22**, 734–738.
- 48 B. M. Sandra, L. L. Angela Inmaculada and V. Miguel, *Anal. Chem.*, 2014, **86**, 12279.
- 49 W. Dai, H. Dong, F. Bunshi, Y. Cao, H. Lu, X. Ma and X. Zhang, *Small*, 2015, **11**, 4158–4164.
- 50 Q. Wang, X. Huang, Y. Long, X. Wang, H. Zhang, R. Zhu, L. Liang, P. Teng and H. Zheng, *Carbon*, 2013, **59**, 192–199.
- 51 C. Yu, Z. Zhu, L. Wang, Q. Wang, N. Bao and H. Gu, *Biosens. Bioelectron.*, 2014, **53**, 142.
- 52 R. S. Swathi and K. L. Sebastian, *J. Chem. Phys.*, 2009, **130**, 086101.
- 53 W. Wei, C. Xu, J. Ren, B. Xu and X. Qu, *Chem. Commun.*, 2012, **48**, 1284–1286.
- 54 X. Wang, C. Wang, K. Qu, Y. Song, J. Ren, M. Daisuke, S. Naoki and X. Qu, *Adv. Funct. Mater.*, 2010, **20**, 3967–3971.
- 55 H. Dong, W. Gao, F. Yan, H. Ji and H. Ju, *Anal. Chem.*, 2010, **82**, 5511.
- 56 H. Swaminathan, V. Ramar and K. Balasubramanian, *J. Phys. Chem. C*, 2017, **121**, 12585–12592.